

Single Step Transformation of Urea into Metal-Free $g\text{-C}_3\text{N}_4$ Nanoflakes for Visible-Light Photocatalytic Degradation of Crystal Violet Dye

M. Nikitha¹, Nagaraju Kottam^{2*}, S. P. Smrithi¹, Bharath K. Devendra¹, S. G. Prasannakumar¹ and G. Prasanth³

¹Department of Chemistry, M S Ramaiah College of Arts, Science and Commerce, MSRIT Post, MSR Nagar, Bengaluru – 560054, Karnataka, India

²Department of Chemistry, M S Ramaiah Institute of Technology (An Autonomous Institute affiliated with Visvesvaraya Technological University, Belagavi), Bengaluru – 560054, Karnataka, India; nagaraju@msrit.edu.in

³Department of Chemical Engineering, M S Ramaiah Institute of Technology (An Autonomous Institute affiliated with Visvesvaraya Technological University, Belagavi), Bengaluru – 560054, Karnataka, India

Abstract

The danger that dyes pose to the biosphere is a worry for the entire planet. So, it is essential to remove these colors using the appropriate methods from the aquatic system. The best and most efficient approach for removing colors from water and wastewater is photodegradation utilizing graphitic carbon nitride ($g\text{-C}_3\text{N}_4$). The photocatalytic activity of the $g\text{-C}_3\text{N}_4$ nanoflakes under visible light was examined in the current work using crystal violet dye. Due to its high efficiency, visible light radiation is typically used to photodegrade dyes. The environmentally benign molecular precursor urea was employed to initiate a single-step pyrolysis procedure that yielded $g\text{-C}_3\text{N}_4$ nanoflakes. The efficiency of the urea conversion process was determined at 550 °C. X-ray diffraction analysis has confirmed the graphitic phase of the synthesized carbon nitride material. The layered structure of the sp^2 hybridized carbon and nitrogen bonding characteristics is confirmed by FT-IR analysis. The synthesized $g\text{-C}_3\text{N}_4$ has a nanosheet like morphology according to HRTEM analysis. $g\text{-C}_3\text{N}_4$ showed enhanced photocatalytic activity resulting in 97 % mineralisation of Crystal Violet (CV) dye and also compared its efficacy with dye concentration. All photocatalytic behavior was analysed by using a UV-Visible spectrophotometer.

Keywords: $g\text{-C}_3\text{N}_4$, HRTEM, Mineralisation, Photocatalysis, Pyrolysis.

1.0 Introduction

Recent years have seen a major exaggeration of the environmental system crisis as a result of the rapid rise of industrialization. Different organic dyes are employed, particularly in industries like textile, cosmetic, paints, tannery, printing in textile industries, and so on^{1,2}. Across the globe, all these dyes are released into the marine atmosphere, where they have teratogenic, carcinogenic,

and mutagenic effects in humans. Destructive organic dyes from the marine atmosphere is therefore essential for the preservation of our ecosystem in order to avoid these risks³⁻⁵. Physical, chemical, and biological methods have all been used in this regard to sanitizing the area where these organic pigments are present⁶⁻⁹.

One of the sustainable energy methods used to decompose organic contaminants is visible light-driven

*Author for correspondence

photocatalysis. Due to their broad intrinsic band gap, conventional semiconductors metal oxide nanoparticles like TiO₂, ZnO, and SnO₂ are UV light active but ineffective for visible light photocatalytic activity. Rapid photoinduced electron-hole pair recombination is another barrier to using these semiconductors as photocatalysts. Carbon nitride which is stable allotrope has a mid-band gap energy of 2.7 eV and that is g-C₃N₄¹⁰. It has 2D stacked conjugated graphitic planes made of carbon and nitrogen atoms that have undergone sp² hybridization¹¹. Since the graphitic phase of C₃N₄ is extremely constant in air up to 600°C, it can be used in applications that need high temperatures¹². Additionally, one of the intriguing options is g-C₃N₄¹³.

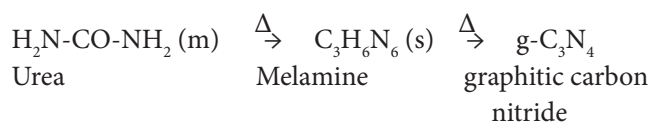
The preparation of g-C₃N₄ from substances including dicyandiamide¹⁴, melamine¹⁵, thiourea¹⁶, urea¹⁷, and trithiocyanuric acid¹⁸ has been described by several researchers. The majority of these precursors are overpriced, destructive, and sometimes even hazardous. Urea is one of the plentiful, inexpensive, and non-toxic precursor compounds.

In the current study, g-C₃N₄ was produced utilizing a single phase of pyrolysis without any pre- or post-treatment, using urea as a precursor. XRD, HRTEM, EDX, and FTIR are a few of the advanced analytical techniques used to create and characterize g-C₃N₄. Additionally, the photodegradation of the produced g-C₃N₄ in response to visible light was investigated for the deterioration/mineralisation of the crystal violet dye.

2.0 Materials and Materials

2.1 g-C₃N₄ Fabrication

A single-step pyrolysis process was used to create g-C₃N₄ utilizing analytical grade urea as a precursor. A typical synthesis procedure involved heating 15 g of urea to 550°C in a muffle furnace for 240 minutes in a crucible that was closed with a lid. The final step involved annealing the resulting product for three hours at 500°C. After the heating process, the furnace was allowed to cool to room temperature. The ash portion that was collected has a light yellow color. The process of g-C₃N₄ formation can be expressed simply as follows.



2.2 Characterization of g-C₃N₄

With a Bruker D8 advance diffractometer outfitted with Cu k alpha radiation with a wavelength of 0.15406 nm, X-ray diffraction tests were performed. The Parkin Elmer Spectrum 1000 was used for the spectral methods of infrared light using the total reflectance attenuated mode. Data from MIRA 3's Field Emission Scanning Electron Microscopy (FESEM) and Quantax 200's energy dispersive X-ray spectroscopy studies (EDS). With double detection and adjustable spectral resolutions, the Specord 210 Plus was used for UV-visible absorption research.

2.3 Photocatalytic Behavior of g-C₃N₄

The photodegradation investigations were carried out using a light source made up of mercury vapor lamp (125 W) in a photocatalytic reactor. Typically, a known amount of photocatalyst was put to the dye solution of known concentration and magnetically agitated for around thirty minutes to let adsorption-desorption equilibrium to be attained between the pollutant dye and the photocatalyst under dark conditions. The solution was then continuously stirred while being exposed to visible light. By continuously noting the absorbance maxima at 591 nm after 2 mL of material was removed periodically without disrupting the apparatus, the concentration of CV dye was analysed.

3.0 Results and Discussion

3.1 XRD Analysis

The graphitic carbon nitride subjected to X-ray diffraction experiments shown in Figure 1 showed a typical intense diffraction peak at 2 theta 27.6 ° that can be indexed to the (002) graphitic plane (PDF#87-1526) indicative of the graphitic interlayer stacking. The graphitic materials' less strong diffraction patterns obtained about 17.7 ° can be attributed to the (100) plane, suggesting the packing of structural motifs in-plane, and are consistent with JCPDS 87-1526¹⁹.

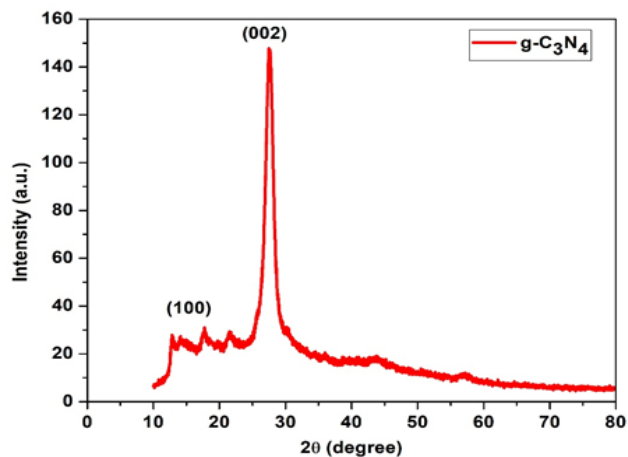


Figure 1. XRD pattern obtained for g-C₃N₄.

3.2 HRTEM and EDX Analysis

Images from high-resolution transmission electron microscopy taken of g-C₃N₄ show that it has a sheet-like appearance comparable to graphene. The synthesized g-C₃N₄ is within the nanoregime in thickness, as shown by Figure 2, and its look is consistent with the literature that is now in circulation. The selected area diffraction (SAED) pattern for g-C₃N₄ showed a diffused ring pattern, suggesting that the substance is amorphous and lacks a clear atomic organization. Additionally, the Energy dispersive elemental analysis (Figure 3) exhibits the carbon and nitrogen-related signals and this justifies the presence of g-C₃N₄.

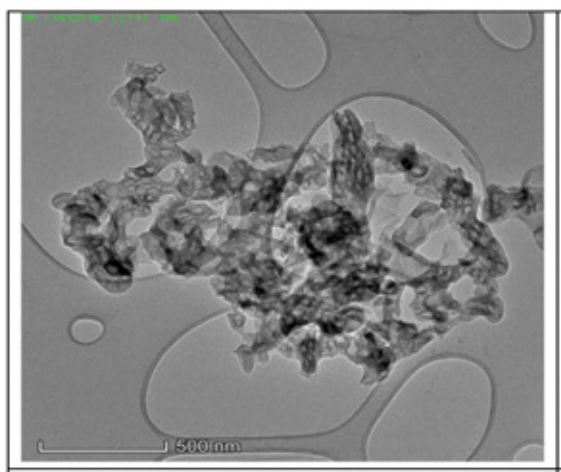


Figure 2. Image of HRTEM of g-C₃N₄.

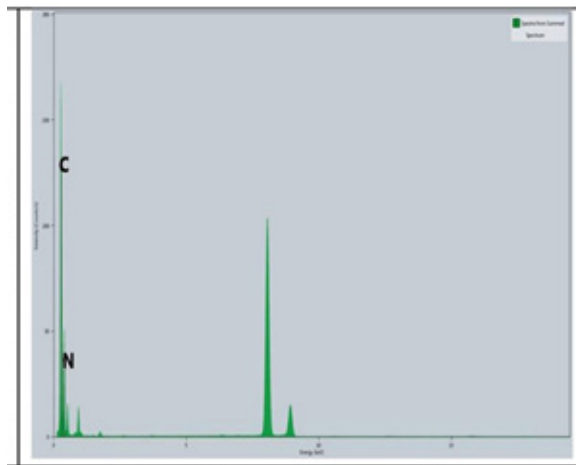


Figure 3. EDX spectrum for g-C₃N₄.

3.3 FTIR Analysis

The stretching mode vibrations of aromatic C-N bonds and C=N heterocycles can be attributed to the bands at 1630, 1563, 1420, 1324, and 1241 cm⁻¹ that are revealed by Fourier transform infrared spectroscopy studies on g-C₃N₄ (Figure 4). The band that began at roughly 808 cm⁻¹ and is attributed to the breathing mode of the heptazine ring structure reflects the intact-well preserved graphitic C-N network. Additionally, the existence of terminal NH₂ showing the N-H stretching vibrations is suggested by the broad band at 3175 cm⁻¹ ^{20,21}.

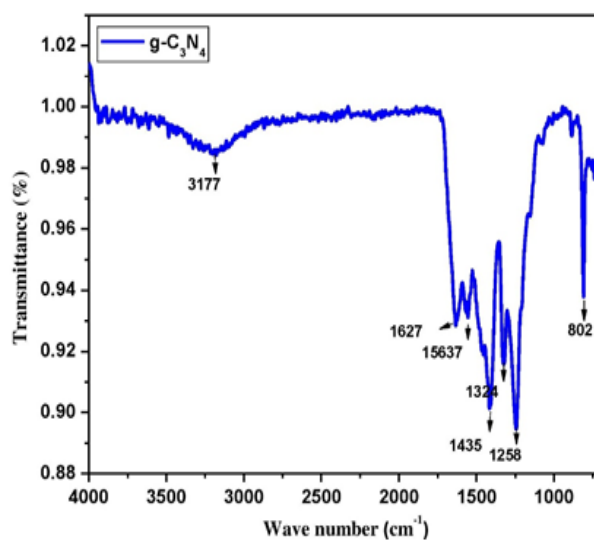


Figure 4. FTIR spectrum of g-C₃N₄.

4.0 Photocatalytic Dye Degradation Activities $g-C_3N_4$

The photocatalytic degradation ability of the synthesized $g-C_3N_4$ for the mineralization of crystal violet dye which is cationic in nature is investigated. A known concentration (10 ppm) of crystal violet dye solution was stirred for uniform concentration, to which 50 mg of the photocatalyst is added and degradation experiments are carried out. The results are depicted in Figure 5 in the form of UV-Visible absorbance spectra of crystal violet dye at different time intervals.

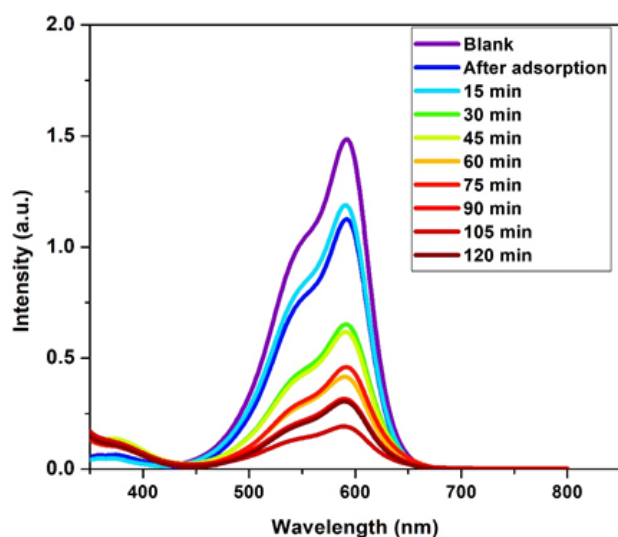


Figure 5. UV-Visible absorbance spectra of CV dye during degradation.

4.1 Effect of Initial Dye Concentration

As CV dye concentration increased, $g-C_3H_4$ catalyst action decreased. The concentration of the dye plays a major role in how quickly it degrades beneath the light source. The study was done in 100 ml with 10 ppm, 20 ppm, 30 ppm, and 40 ppm dye concentrations to find the ideal dye concentration, which is depicted in (Figures 6). This depends on how dense the dye molecules are on the catalytic surface, which limits the amount of light that can flow through the catalyst and slows dye breakdown as a result. As a result, it was discovered that there was a decrease in the rate of hydroxyl and superoxide radical formation. The 10 ppm finding shows that higher dye concentrations are related to more photocatalytic

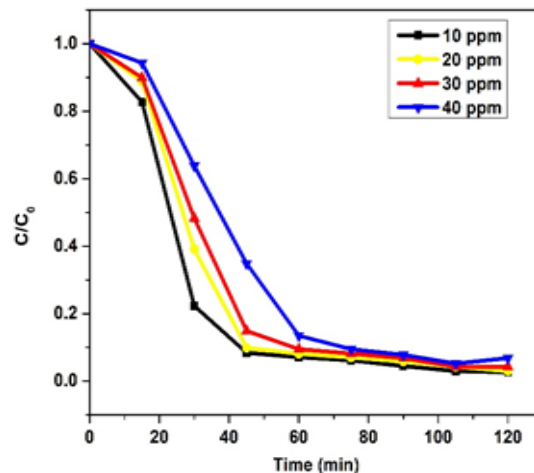


Figure 6. Degradation studies of CV dye at different concentrations.

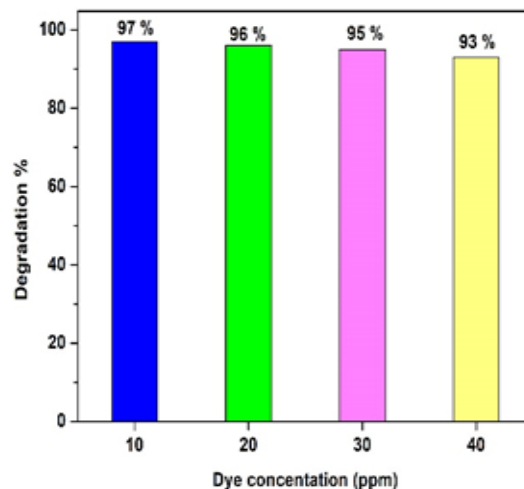


Figure 7. Dye degradation percentage for 50mg catalyst.

degradation. (10–20 ppm). The exact dye degradation efficiency for different dye concentrations is clearly expressed in (Figure 7).

5.0 Feasible Procedure of Dye Degradation

Here, the photocatalytic mechanism has been succinctly presented. Figure 11 illustrates how photon energy has fallen to the surface. When $g-C_3H_4$ were exposed to photons, the presence of electrons (e^-) in the valence band (VB) stimulated the conduction band (CB) with

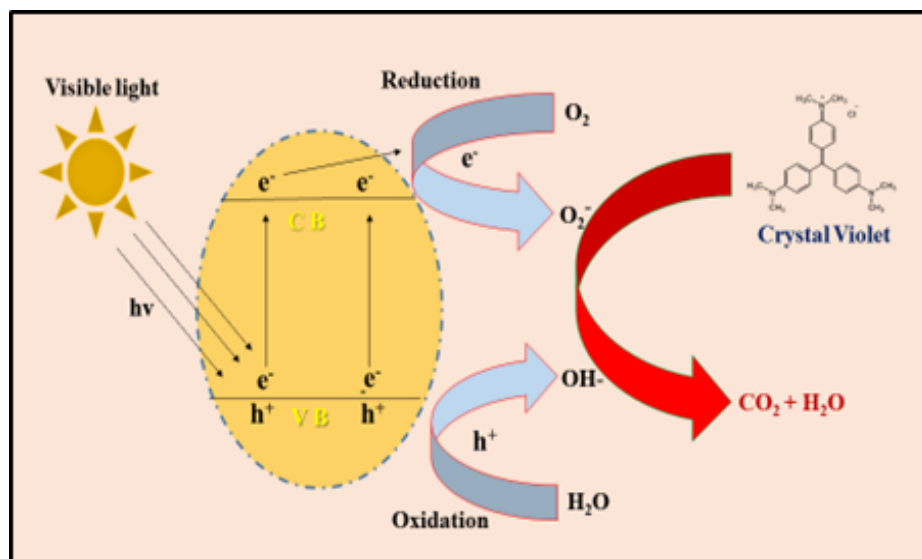
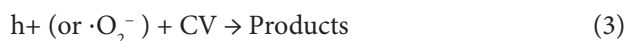
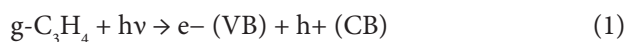


Figure 8. Mechanism of photocatalyst degradation for CV dye shown schematically.

the identical number of holes (h^+) lasting in the VB²³⁻²⁵. While photogenerated h^+ oxidizes CV dye on the surface of $g-C_3N_4$ samples, photogenerated electrons (e^-) combine with O_2 to produce $O_2^{\cdot-}$. The CV dye molecules could then be significantly reduced by these potent oxidants to H_2O , CO_2 , and other insignificant molecules (Figure 8). It was hypothesized that CV may undergo photocatalytic degradation over $g-C_3N_4$ samples.



6.0 Conclusion

In our current research, urea was used as an environmentally safe starting material to create $g-C_3N_4$ nanoflakes. Numerous characterization methods, including HRTEM, EDX, XRD and FTIR, have been used to validate successful growth of the sample. The synthesized sample's 2.7 eV bandgap makes it appropriate for photocatalytic applications that respond to visible light. Surprisingly, the $g-C_3N_4$ could degrade CV dye to the extent of 97%. The photocatalytic activity has been demonstrated at different dye concentrations as CV dye concentration increased,

$g-C_3N_4$ catalyst action decreased. The breakdown of CV dye by photocatalysis when exposed to visible light suggests that $g-C_3N_4$ nanoflakes are suitable for treating pollutants. Overall, $g-C_3N_4$ sample will eventually replace the current techniques for waste management and water disinfection.

7.0 References

- Asadzadeh-Khaneghah S, Habibi-Yangjeh A, Nakata, K. Decoration of carbon dots over hydrogen peroxide treated graphitic carbon nitride: Exceptional photocatalytic performance in removal of different contaminants under visible light. *J Photochem Photobiol A: Chem.* 2019; 374:161-72. <https://doi.org/10.1016/j.jphotochem.2019.02.002>
- Bahuguna A, Choudhary P, Chhabra T, Krishnan V. Ammonia-doped polyaniline-graphitic carbon nitride nanocomposite as a heterogeneous green catalyst for synthesis of indole-substituted 4 H-chromenes. *ACS Omega.* 2018; 3(9):12163-78. <https://doi.org/10.1021/acsomega.8b01687> PMID:31459291 PMCID: PMC6645668
- Nair SSP, Kottam N, Prasannakumar SG. Green synthesized luminescent carbon nanodots for the sensing application of Fe^{3+} ions. *J Fluoresc.* 2020; 30(2):357-63. <https://doi.org/10.1007/s10895-020-02505-2> PMID: 32076915

4. Che H, Liu L, Che G, Dong H, Liu C, Li C. Control of energy band, layer structure and vacancy defect of graphitic carbon nitride by intercalated hydrogen bond effect of NO₃⁻ toward improving photocatalytic performance. *Chem Eng J.* 2019; 357:209-29. <https://doi.org/10.1016/j.cej.2018.09.112>
5. Wang Q, Shi Y, Pu L, Ta Y, He J, Zhang S, *et al.* Fabrication of the carnation-like CCN-CuS p-n heterojunctions with enhanced photocatalytic performance under visible light irradiation. *Appl Surface Sci.* 2016; 367:109-17. <https://doi.org/10.1016/j.apsusc.2016.01.148>
6. Smrithi SP, Kottam N, Arpitha V, Narula A, Anilkumar GN, Subramanian KRV. Tungsten oxide modified with carbon nanodots: integrating adsorptive and photocatalytic functionalities for water remediation. *J Sci: Adv Mater Dev.* 2020; 5(1):73-83. <https://doi.org/10.1016/j.jsamd.2020.02.005>
7. Wang M, Jin C, Li Z, You M, Zhang Y, Zhu, T. The effects of Bismuth (III) doping and ultrathin nanosheets construction on the photocatalytic performance of graphitic carbon nitride for antibiotic degradation *J Colloid and Interface Sci.* 2019; 533: 513-25. <https://doi.org/10.1016/j.jcis.2018.08.113> PMID:30179830
8. Devendra BK, Praveen BM, Tripathi VS, Nagaraju G, Prasanna BM, Shashank M. Development of rhodium coatings by electrodeposition for photocatalytic dye degradation. *Vacuum.* 2022; 205. <https://doi.org/10.1016/j.vacuum.2022.111460>
9. Wang Y, Li Y, Cao S, Yu J. Ni-P cluster modified carbon nitride toward efficient photocatalytic hydrogen production. *Chinese J Catal.* 2019; 40(6):867-74. [https://doi.org/10.1016/S1872-2067\(19\)63343-7](https://doi.org/10.1016/S1872-2067(19)63343-7)
10. Smrithi SP, Kottam N, Narula A, Madhu GM, Mohammed R, Agilan, R. Carbon dots decorated cadmium sulphide heterojunction-nanospheres for the enhanced visible light driven photocatalytic dye degradation and hydrogen generation *J Colloid Interface Sci.* 2022; 627:956-68. <https://doi.org/10.1016/j.jcis.2022.07.100> PMID:35901574
11. Zheng Y, Liu J, Liang J, Jaroniec M, Qiao SZ. Graphitic carbon nitride materials: Controllable synthesis and applications in fuel cells and photocatalysis. *Energy and Environ Sci.* 2012; 5(5):6717-31. <https://doi.org/10.1039/c2ee03479d>
12. Zhu J, Xiao P, Li H, Carabineiro SA. Graphitic carbon nitride: Synthesis, properties, and applications in catalysis. *ACS Appl Mater Interfaces.* 2014; 6(19):16449-65. <https://doi.org/10.1021/am502925j> PMID:25215903
13. Dong G, Zhang Y, Pan Q, Qiu J. A fantastic graphitic carbon nitride (g-C₃N₄) material: Electronic structure, photocatalytic and photoelectronic properties. *J Photochem Photobiol C: Photochem Rev.* 2014; 20:33-50. <https://doi.org/10.1016/j.jphotochemrev.2014.04.002>
14. Rathod MR, Rajappa SK, Praveen BM, Bharath DK. Investigation of Dolichandra unguis-cati leaves extract as a corrosion inhibitor for mild steel in acid medium. *Curr Res Green Sustain Chem.* 2021; 4. <https://doi.org/10.1016/j.crgsc.2021.100113>
15. Fang J, Fan H, Li M, Long C. Nitrogen self-doped graphitic carbon nitride as efficient visible light photocatalyst for hydrogen evolution. *J Mater Chem A.* 2015; 3(26):13819-26. <https://doi.org/10.1039/C5TA02257F>
16. Smrithi SP, Kottam N, Vergis BR. Heteroatom modified hybrid carbon quantum dots derived from Cucurbita pepo for the visible light driven photocatalytic dye degradation. *Top Catal.* 2022; 1-12. <https://doi.org/10.1007/s11244-022-01581-x>
17. Yuan YP, Xu WT, Yin LS, Cao SW, Liao YS, Tng YQ, *et al.* Large impact of heating time on physical properties and photocatalytic H₂ production of g-C₃N₄ nanosheets synthesized through urea polymerization in Ar atmosphere. *Int Hydrog Ener.* 2013; 38(30):13159-63. <https://doi.org/10.1016/j.ijhydene.2013.07.104>
18. Chen J, Hong Z, Chen Y, Lin B, Gao B. One-step synthesis of sulfur-doped and nitrogen-deficient g-C₃N₄ photocatalyst for enhanced hydrogen evolution under visible light. *Mater Lett.* 2015; 145:129-32. <https://doi.org/10.1016/j.matlet.2015.01.073>
19. Devendra BK, Praveen BM, Tripathi VS, Nagaraju G, Nagaraju DH, Nayana KO. Highly corrosion resistant platinum-rhodium alloy coating and its photocatalytic activity. *Inorg Chem Commun.* 2021; 134. <https://doi.org/10.1016/j.inoche.2021.109065>
20. Wang X, Blechert S, Antonietti M. Polymeric graphitic carbon nitride for heterogeneous photocatalysis. *ACS Catal.* 2012; 2(8):1596-606. <https://doi.org/10.1021/cs300240x>
21. Devendra BK, Praveen BM, Tripathi VS, Kumar HP, Chethana KR. The development of platinum-rhodium alloy coatings on SS304 using a pulse/direct electrodeposition technique and their application to antibacterial activity. *J Indian Chem Soc.* 2022; 99(6). <https://doi.org/10.1016/j.jcis.2022.100466>
22. Zhang G, Zhang J, Zhang M, Wang X. Polycondensation of thiourea into carbon nitride semiconductors as visible

- light photocatalysts. *J Mater Chem.* 2012; 22(16):8083-91. <https://doi.org/10.1039/c2jm00097k>
23. Archana B, Kottam N, Smrithi SP, Sekhar KBC. Fabrication of 2D+ 1D nanoarchitecture for transition metal oxide modified CdS nanorods: A comparative study on their photocatalytic hydrogen-generation efficiency. *Nanotechnology.* 2023; 34(44). <https://doi.org/10.1088/1361-6528/acec50> PMID:37527631
24. Sharieff S, Veluturla S, Kottam N, Smrithi SP, Singhvi R. Esterification of levulinic acid to butyl levulinate over $\text{TiO}_2/\text{WO}_3/\text{SO}_4^{2-}$: Optimization and kinetic study. *Biomass Convers Biorefin.* 2023; 1-15. <https://doi.org/10.1007/s13399-023-04016-z>
25. Gurushantha K, Kottam N, Smrithi SP, Dharmaprasanth MS. Visible light active WO_3/TiO_2 heterojunction nanomaterials for electrochemical sensor, capacitance and photocatalytic applications. *Catal Lett.* 2023; 1-12. <https://doi.org/10.1007/s10562-023-04362-7>